Journal of The Electrochemical Society, **159** (5) K122-K126 (2012)
0013-4651/2012/159(5)/K122/5/$28.00 © The Electrochemical Society

Microstructural Properties and Formation Mechanisms of Zn Nanocrystal Embedded Polydimethylsiloxane Nanofibers

Jae Won Shin,[a] Dae Jin Yang,[b] Yong-Woon Jang,[c] Byung Cheol Lee,[d] Woo Seung Song,[e] Jin-Gyu Kim,[a] Seong Jo Yoo,[a] Jeong Yong Lee,[c] Il-Doo Kim,[c] Dea Uk Lee,[e] Seok-Hoon Lee,[a] and Tae Whan Kim[e,z]

[a]*Division of Electron Microscopic Research, Korea Basic Science Institute (KBSI), Daejeon 305-333, Korea*
[b]*Department of Materials and Engineering, Massachusetts Institute of Technology, Cambridge, Massachusetts 02139, USA*
[c]*Department of Materials Science and Engineering, KAIST, Daejeon 305-701, Korea*
[d]*Laboratory For Quantum Optics, Korea Atomic Energy Research Institute, Daejeon 305-600, Korea*
[e]*National Research Laboratory for Nano Quantum Electronics Devices, Department of Electronics and Computer Engineering, Hanyang University, Seoul 133-791, Korea*

The silicone-sheathed nanofibers based on ZnO-SiO_x nanofibers transformed into Zn nanocrystal embedded polydimethylsiloxane (silicone) nanofibers by using electron-beam irradiation. Transmission electron microscopy (TEM) images showed that silicone-sheathed ZnO-SiO_x nanofibers were synthesized during electron-beam irradiation of the calcined ZnO-SiO_x nanofiber. High-resolution TEM image showed that the nanofibers were transformed into Zn nanocrystal embedded silicone nanofibers. The structural variation of the nanofibers was attributed to the evaporation and deposition of the silicone molecule and to the thermodynamic and double ionization effects during electron beam irradiation. The Zn nanocrystal embedded silicone nanofibers were formed due to the oxidation and the reduction due to the thermal and double ionization effects at the later stage of the electron-beam irradiation.
 [DOI: 10.1149/2.050205jes]

Manuscript submitted December 12, 2011; revised manuscript received February 3, 2012. Published February 28, 2012.

One-dimensional (1D) nanocomposites have attracted a great deal of interest due to their particular physical properties and potential applications in sensors, solar cells, transistors, nanogenerators, and multifunctional electronics.[1–4] The prospect of potential applications of electronic and optoelectronic devices fabricated utilizing 1D nanocomposites has led to substantial research and development efforts on surface modification, structural engineering, and compositional control.[5–7] Among the various kinds of 1D nanocomposites, 1D core-shell and encapsulation systems of semiconductors or metal nanocrystals surrounded by an insulating layer have become particularly attractive because of their promising applications in next-generation electronic and optoelectronic devices.[8–10] The sol-gel process, co-sputtering deposition, thermal evaporation, chemical vapor deposition, pulsed laser deposition, ion implantation, and irradiation-induced modification method have been used to form such types of nannocomposites.[11–15]

The electron-beam irradiation process in a transmission electron microscope (TEM) induces a structural transformation of the Zn-Si-O thin film to metallic Zn nanocrystals in a SiO_2 matrix.[16,17] Even though some works concerning the formation and the physical properties of Zn nanocrystals embedded in an insulating layer have been conducted,[17] comprehensive studies on the formation mechanisms of Zn nanocrystals inserted in polydimethylsiloxane (silicone) nanofibers by using electrospinning and electron-beam irradiation have not been reported yet. Furthermore, nanocomposites containing metal nanocrystals embedded in silicone nanofibers have emerged as excellent candidates for potential applications in next-generation electronic devices because of their excellent advantages of flexibility, high chemical stability, and high self-healing ability.[18–20]

Transmission electron microscopy (TEM) and selected area electron diffraction pattern (SADP) measurements were carried out to investigate the microstructural properties of the polymeric sheath, the ZnO and the Zn nanocrystals embedded in the nanofiber. Energy dispersive spectroscopy (EDS) and electron energy loss spectroscopy (EELS) measurements were performed to investigate the stoichiometries of the polymeric sheath and the ZnO-SiO_x nanofibers. The transformation mechanisms from the electrospun metal-oxide semiconductor nanofibers to the silicone-sheathed nanofibers and the formation mechanisms of the metal nanocrystal embedded silicone nanofibers are described on the basis of the high-resolution TEM (HRTEM) images, the EELS mapping, and the EDS profiles.

Experimental Details

The ZnO-SiO_x nanofibers used in this study were formed by using an electrospinning technique. ZnO-SiO_x nanofibers have been receiving considerable attention for promising applications in catalysts, gas sensors, field-effect transistors, transparent optical devices, and photoelectrochemical cells.[21] The SiO_x surface of the metal-oxide semiconductor in the absorption/emission range is optically transparent, and the surface has excellent functions with attachment of biomolecule ligands.[22] The ZnO-SiO_x nanofibers were transformed by irradiating them with an electron beam from an electron accelerator (300 keV and 1.5 mA). Electrospinning is one of the simplest, most versatile, and lowest-cost methods for producing long continuous fibers with typical diameters ranging from 50 nm up to few micrometers and with lengths of up to several centimeters. The formation of the hybrid inorganic-organic nanocomposites is challenging due to the controllable mixing of the materials.[23] The method used in this study overcomes the disadvantage of electrospinning by combining it with electron-beam irradiation. In particular, the electron accelerator was operated at room temperature and in the atmosphere, and the operator could uniformly inject electrons into a sample with a very large are of 20 cm × 20 cm.[24]

The precursor solution was prepared by dissolving zinc acetate (0.84 g), tetraethyl orthosilicate (TEOS, 0.84 mL), and polyvinylpyrrolidone (PVP, $(C_6H_9N_O)_n$, 0.8 g) in a mixture of dimethyl formamide (DMF, 7.5g) and acetic acid. DMF was used as a solvent, and acetic acid was added to ensure a mixed solution with a high conductivity. The precursor solution was transferred into a syringe and injected through a stainless steel needle, which was connected to a high-voltage DC power supply. The solution was continuously fed at a constant and controllable rate by using a syringe pump (KD Scientific, 781200). A high voltage of 13 kV was applied between the needle tip and the stainless steel substrate, resulting in the jetting of a continuous fiber stream, as shown in Fig. 1a. The distance between the needle tip and the substrate was 30 cm, and the feeding rate of the precursor solution was 1 μL/min. An adequate distance between the tip and the collector electrode is required to allow the solvent to evaporate during electrospinning. While the distance between the tip and the counter electrode is 10–25 cm in laboratory systems

[z] E-mail: twk@hanyang.ac.kr

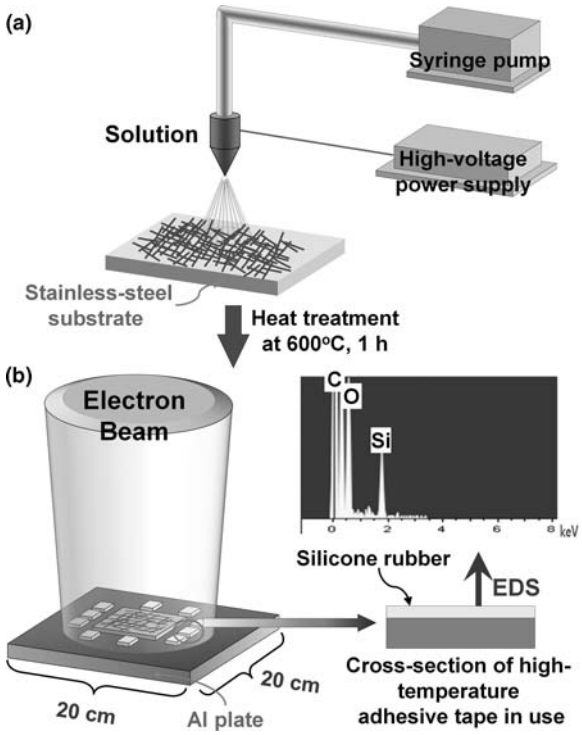

Figure 1. Schematic diagrams of (a) the fabrication and (b) the electron beam irradiation processes for the nanofiber.

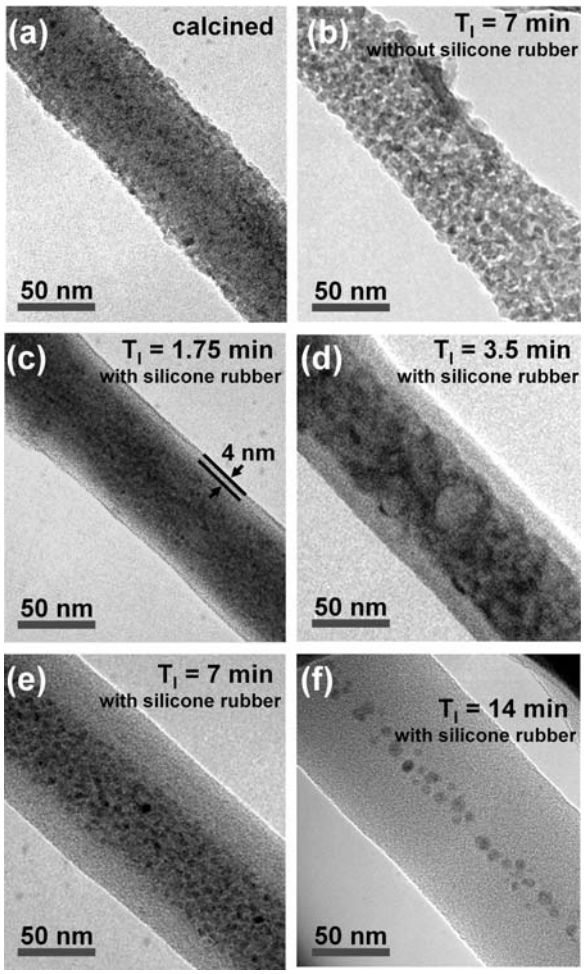

Figure 2. The bright-field TEM images of (a) a calcined Zn-Si-O nanofiber with a diameter of approximately 70 nm formed by using an electrospinning method, (b) a Zn-Si-O nanofiber without silicone rubber and electron irradiated for 7 min, and Zn-Si-O nanofibers with silicone rubber and electron irradiated for (c) 1.75, (d) 3.5, (e) 7, and (f) 14 min.

under normal circumstances,[25] the formation distance for nanofibers without beads in this electrospinning system is 30 cm. Subsequently, the as-spun fibers were calcined at 600°C for 1 h in air in order to crystallize the inorganic components and to remove the solvent and the polymers. The sample with or without silicone rubber (polydimethyl siloxane, $[SiO(CH_3)_2]_n$), which is taken off adhesive film of silicone adhesion tape, was placed, on an aluminum stage. Then, an electron irradiation process was carried out by using an electron accelerator, as shown in Fig. 1b. The electron energy of the electron accelerator was 300 keV, and its average current was 1.5 mA. The adhesive film was composed of silicone, polymer containing silicon (Si), carbon (C), hydrogen (H), and oxygen (O), as confirmed by the EDS spectra of the adhesive film shown in the inset of Fig. 1b.

The nanofiber was taken off the substrate by using ultrasonications in acetone, methanol and distilled water at 60°C for 15 min and was then rinsed in de-ionized water thoroughly. After chemical cleaning, the nanofiber-loaded solution was spread on a TEM Cu grid for TEM, EDS and EELS measurements. The Bright field TEM and HRTEM measurements were performed using a JEM-ARM 1300S high voltage EM (HVEM) and F30 S-twin field-emission TEM (FE-TEM), operating at 1250 and 300 kV, respectively. The EELS and EDS measurements were performed using post-column energy filter (HV-GIF 2000, Gatan) attached to JEM-ARM 1300S and EDS System (Genesis, EDAX) attached to F30 S-twin, respectively.

Results and Discussion

Figure 2 shows bright-field TEM images of (a) a calcined Zn-Si-O nanofiber with a diameter of approximately 70 nm formed by using an electrospinning method and of (b) a Zn-Si-O nanofiber without silicone rubber and electron irradiated for 7 min and of Zn-Si-O nanofibers with silicone rubber and electron irradiated for (c) 1.75, (d) 3.5, (e) 7, and (f) 14 min. When the Zn-Si-O nanofibers are formed by using the electrospinning method, ZnO nanocrystals are embedded in an amorphous SiO_x matrix with a rough surface, as shown in Fig. 3a, which is a high-magnification image of Fig. 2a. When the calcined ZnO-SiO_x nanofibers without silicone rubber were irradiated by using electrons for 7 min, the electrons directly interacted with the atoms of ZnO-SiO_x nanofibers, resulting in knock-on displacement, E-beam sputtering, and heating.[26] Consequently, because the ZnO nanocrystals embedded in the amorphous SiO_x matrix transformed into Zn or Zn-Si-O compounds in the nanofiber, they are fragile and aggregated, resulting in the formation of a rougher surface in comparison with the calcined nanofiber. Silicone-sheathed nanofibers were synthesized during electron-beam irradiation with silicone rubber, as shown in Figs. 2c–2e. Silicone-sheathed nanofibers or Zn nanocrystals embedded in the silicone nanofibers were uniformly coated on the sample. The silicone-sheath nanofibers with an optimal structure have better thermal stability and extremely wetting characteristics due to the super hydrophobic surface in comparison with the nanofibers without sheath and conventional polymeric sheath nanofiber.[27] The thickness of the silicone sheath could be precisely controlled by using the electron-beam irradiation. Furthermore, the surface of the silicone-sheathed nanofibers formed by using the electron-beam irradiation method was smoother than that of the calcined nanofiber, as shown in Figs. 2c–2e.

The HRTEM images show the edge of the (a) calcined ZnO-SiO_x nanofiber and (b) silicone-sheathed ZnO-SiO_x nanofibers formed by using the electron beam irradiation for 3.5 min in Figs. 3a and 3b, respectively, indicating that the nanofibers have very smooth surfaces after electron-beam irradiation for 3.5 min with silicone rubber.

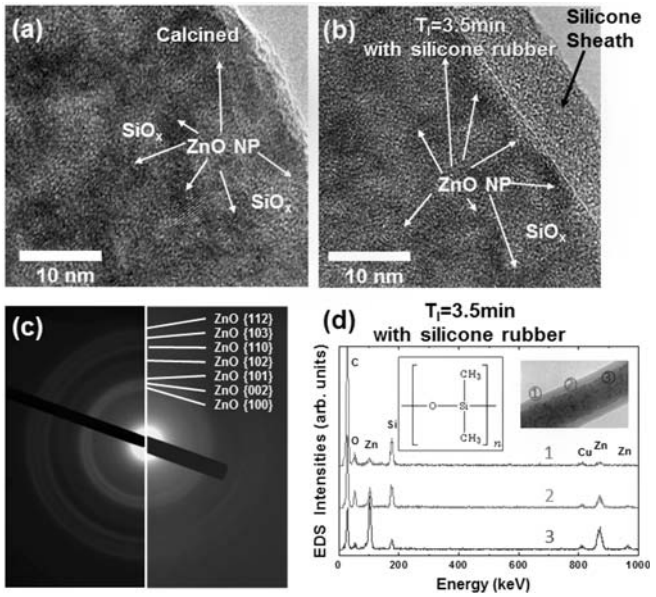

Figure 3. (a) HRTEM image of the edge of a calcined ZnO-SiO_x nanofiber, and of (b) a ZnO-SiO_x nanofiber that had been electron-irradiated for 3.5 min, and (c) a SADP images taken from a calcined ZnO-SiO_x nanofiber (left side) and silicone-sheathed ZnO-SiO_x nanofibers formed by using the electron beam irradiation for 3.5 min (right side), and (d) EDS spectra taken from areas 1, 2, and 3 of the inset of the bright-field TEM image and the chemical structure of PDMS.

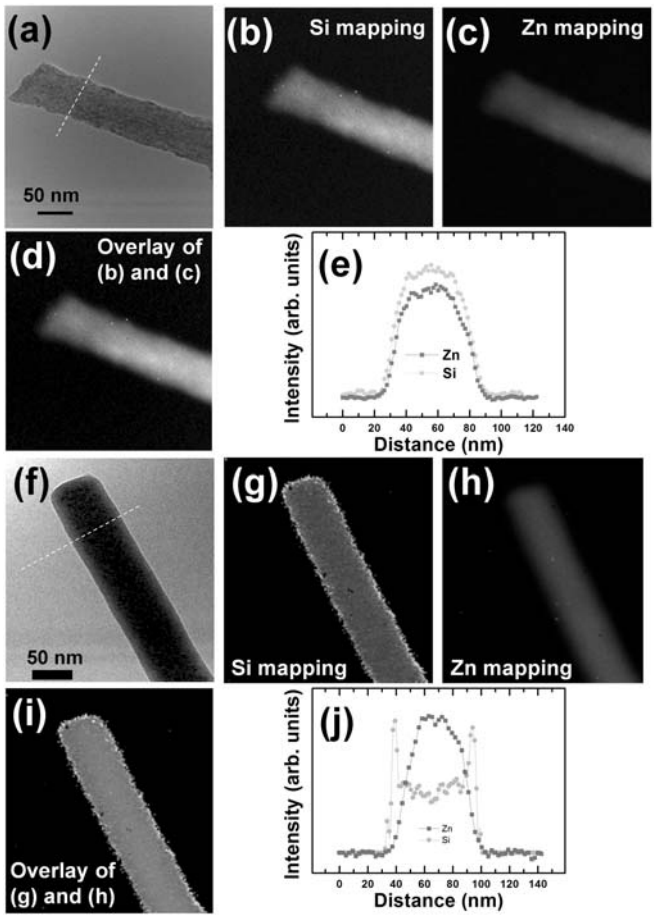

Figure 4. (a) and (f) bright-field TEM images, (b) and (g) element mapping images of Si, (c) and (h) element mapping images of Zn, (d) and (i) overlay of Si and Zn mapping images, and (e) and (j) elemental analyzes of the EELS line profiles of the calcined ZnO-SiO_x nanofiber and the silicone-sheathed ZnO-SiO_x nanofiber by using electron-beam irradiation for 3.5min. The Si and the Zn signals are indicated as the green and the red colors, respectively.

SADP images taken from a calcined ZnO-SiO_x nanofiber (left side) and silicone-sheathed ZnO-SiO_x nanofibers formed by using the electron beam irradiation for 3.5 min (right side) have almost same ring patterns, as shown in Fig. 3c. The SAPD images show that the embedded nanocrystals in ZnO-SiO_x nanofibers and silicone-sheathed ZnO-SiO_x nanofibers had the same wurtzite structure of ZnO nanocrystals, indicating that ZnO-SiO_x nanofibers maintain their original crystalline structure during an initial stage of the electron beam irradiation. Figure 3d, which shows the EDS spectra taken from areas 1, 2, and 3 in the inset of the bright-field TEM image of silicone-sheathed ZnO-SiO_x electron irradiated for 3.5 min, indicating that the silicone-sheathed ZnO-SiO_x nanofibers are well formed. The high intensities of the silicon (Si), oxygen (O), and carbon (C) peaks of the EDS spectrum from area 1 are attributed to the silicone (polydimethylsiloxane; PDMS). The chemical structure of the PDMS shown in the inset of Fig. 3d indicates that the PDMS contains silicon (Si), together with carbon (C), hydrogen (H), and oxygen (O) and that the Cu peak is related to the copper grid.

Elemental mapping analyzes for the calcined ZnO-SiO_x nanofiber and for the silicone-sheathed ZnO-SiO_x nanofiber formed by using electron-beam irradiation for 3.5min have been performed. Figures 4a and 4f show the bright-field TEM images, and Figs. 4b and 4g present the element mappings of Si. Figures 4c and 4h show the element mappings of Zn, and Figs. 4d and 4i depict the superposition of Si (green) and Zn (red) for the calcined ZnO-SiO_x nanofiber and the silicone-sheathed ZnO-SiO_x nanofiber. The elemental analyzes of the EELS line profiles are shown in Figs. 4e and 4j. While the nanofiber without sheath contains Si and Zn atoms in the same region, as shown in Fig. 4e, the silicone-sheath nanofiber consists of Si and Zn atoms in the different region. The existence of large amount of Si atoms formed at the outer regions of the silicone-sheath nanofiber clearly appears, as shown in Figs. 4j. These results are in reasonable agreement with the EELS mapping data.

When an electron beam irradiates the Al plate, as shown in Fig. 1b, the silicone molecules are evaporated into a vapor state by separating them from the solid state of the silicone rubber by breaking the bonds between molecules. The vapor state of the silicone molecules is condensed by depositing silicone molecules on the surface of the nanofiber, resulting in the formation of the silicone sheath for the ZnO-SiO_x nanofiber. Even though the formation mechanism of the silicone sheath is similar to that of physical vapor deposition, the silicone sheath in this experiment was formed in the atmosphere at room temperature.

Figure 5a shows a high-resolution TEM (HRTEM) image of the Zn nanocrystals embedded in a silicone matrix, which is a magnification of Fig. 2f. The SADP of the Zn nanocrystals is indexed as a wurtzite structure, as shown in the inset of Fig. 5a. The weak diffused rings of the SAED pattern are attributed to the amorphous silicone, including a residual SiO_x matrix, or to the small particle size. Figure 5b shows the FFT filtered HRTEM image by masking $\{101\}_{Zn}$ reflections taken from the square area in Fig. 5a. The HRTEM image is obtained by removing the background noise due to the trapping or the scattering of electrons in the amorphous silicone, including a residual SiO_x matrix, surrounding the Zn nanocrystals. These results indicate that the silicone-sheathed ZnO-SiO_x nanofiber is transformed into Zn nanocrystal embedded silicone nanofibers.

The transformation from ZnO nanocrystals in a ZnO-SiO_x nanofiber into Zn nanocrystals embedded in a silicone nanofiber can be described on the basis of the experimental results. First, because the free energy for SiO_2 formation at ~900°C is much smaller than that of ZnO formation, SiO_2 is thermodynamically much more stable than ZnO.[28,29] Therefore, when the oxygen atoms interact with Si and Zn atoms, SiO_2 formation is more intense than ZnO formation due

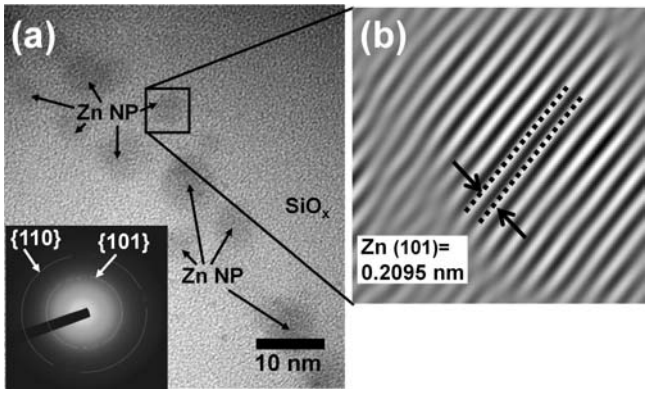

Figure 5. (a) HRTEM image of Zn nanocrystals embedded in silicone nanofibers, including residual SiO_x, which is a magnification of Fig. 2f. The inset is a SAED pattern taken from a Zn-Si-O nanofiber that had been electron irradiated for 14 min. (b) FFT filtered HRTEM image of the rectangular area in Fig. 5a, with masking $\{101\}_{Zn}$ reflections, which was obtained by removing the background noise.

to the larger free energy for SiO_2 formation. The deposition or the reaction of the SiO_2 or the ZnO thin film does not always produce stoichiometric oxygen contents with the production of substoichiometric oxides. Similarly, the suboxide SiO_x layer prefers to take oxygen from the ZnO_x and to oxidize into a thermodynamically stable SiO_2 layer, resulting in a transformation of ZnO_x into metallic Zn in this process.[16]

Secondly, the subsequent excitation process caused by the electron beam might generate two holes in the valence band due to the double ionization effect,[30] resulting in a neutralization of the O^{2-} ions. Zn^{2+} ions are released from the network bonding due to the neutralization of the O^{2-} ions. Because the emitted Zn^{2+} ions capture secondary or Auger electrons existing in the illuminated area due to the induced electrostatic interaction, the Zn^{2+} ions become neutralized to Zn^0 due to the kinetic energy transferred from the electrons,[16] resulting in the O-O bond formation of O_2 gas.[17,31,32] Based on this result, the one-dimensional array structure of the dense ZnO nanocrystals in the ZnO-SiO_x nanofiber is transformed into zero-dimensional well-isolated Zn nanocrystals embedded in a nanofiber, which is caused by the decrease in the volume due to the deoxidation.

Even though the formation mechanisms of Zn nanocrystal embedded silicone nanofibers by using electrospinning and electron-beam irradiation might contribute to a probably quite complicated process, the transformation mechanisms of a ZnO-SiO_x nanofiber into Zn nanocrystal embedded silicone nanofibers could be described on the basis of the TEM images, and the SADP, the EDS profiles, the EELS mappings, and the EELS profiles. After the Zn-Si-O nanofiber is calcined at 600°C, because ZnO-SiO_x compositions are the most stable at high temperature,[33] ZnO-SiO_x nanofibers are formed, as shown in Fig. 6a. When an electron beam irradiate the ZnO-SiO_x nanofibers and the silicone rubber on the Al plate, a silicone sheath is formed on the surfaces of the ZnO-SiO_x nanofibers due to the evaporation and the deposition of silicone molecules on the surfaces of the ZnO-SiO_x nanofibers, as shown in Fig. 6b. However, the silicone-sheathed ZnO-SiO_x nanofiber is transformed into Zn nanocrystal embedded silicone nanofibers, as shown in Fig. 6c, resulting from the oxidation and the reduction due to the thermal and the double ionization effects at the later stage of the electron-beam irradiation.

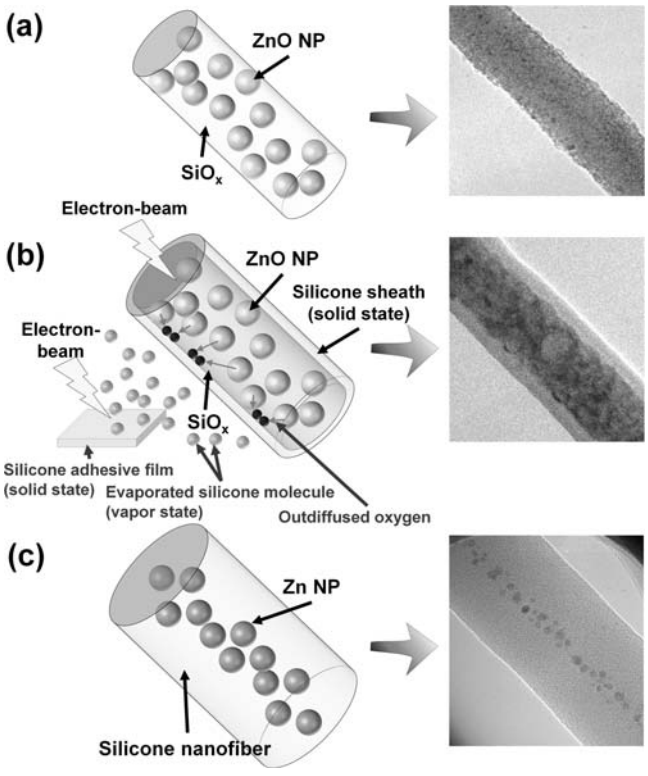

Figure 6. Schematic diagrams, and their corresponding transmission electron microscopy images, for the transformation mechanism of a calcined nanofiber into a silicone-sheathed nanofiber, and Zn nanocrystal embedded silicone nanofibers during electron-beam irradiation.

Conclusions

Zn nanocrystal embedded silicone nanofibers were formed by using electrospinning and electron-beam irradiation with silicone rubber by using an electron accelerator (300 keV and 1.5 mA) for 14 min. Silicone-sheathed ZnO-SiO_x nanofibers were synthesized during electron-beam irradiation of the calcined ZnO-SiO_x nanofibers and silicone rubber due to the evaporation and deposition of silicone molecule at the initial stage of the process. The silicone-sheathed ZnO-SiO_x nanofibers were transformed into Zn nanocrystal embedded silicone nanofibers due to thermodynamic and double ionization effects during the electron-beam irradiation. Bright-field TEM images, HRTEM images, EDS profiles, EELS spectra, and FFT results for the HRTEM images showed that silicone-sheathed ZnO-SiO_x nanofibers were formed and that Zn nanocrystals existed in the silicone nanofibers. The formation mechanisms of silicone-sheathed ZnO-SiO_x nanofibers and of Zn nanocrystals embedded silicone nanofibers are described on the basis of the bright-field TEM images, the HRTEM images, the SADP results, the EDS profiles, and the EELS spectra. Zn nanocrystal embedded silicone nanofibers hold promise for potential fabrication applications in flexible electronic devices.

Acknowledgments

This work was supported by the National Research Foundation of Korea (NRF) grant funded by the Korea Government (MEST) (No. 2010-0018877, No. 2008-2001909). This work also supported by the Korea Basic Science Institute grant (T3121B).

References

1. B. Tian, X. Zheng, T. J. Kempa, Y. Fang, N. Yu, G, Yu, J. Huang, and C. M. Liever, *Nature*, **449**, 885 (2007).
2. Y. B. Tang, Z. H. Chen, H. S. Song, C. S. Lee, H. T. Cong, H. M. Cheng, W. J. Zhang, I. Bello, and S. T. Lee, *Nano Lett.*, **8**, 491 (2008).
3. Z. L. Wang, *Mater. Sci. Eng. R-Rep.*, **64**, 33 (2009).
4. B. P. Timko, T. Cohen-Karai, G. Yu, Q. Qing, B. Tian, and C. M. Lieber, *Nano Lett.*, **9**, 914 (2009).
5. A. Nduwimana and X. Q. Wang, *Nano Lett.*, **9**, 283 (2008).
6. F. Li, S. H. Cho, D. I. Son, T. W. Kim, S-K. Lee, Y-H. Cho, and S. Jin, *Appl. Phys. Lett.*, **94**, 111906 (2009).
7. J. J. Wu, Y. R. Chen, W. P Liao, C. T. Wu, and C. Y. Chen, *ACS Nano*, **4**, 5679 (2010).

8. L. J. Lauhon, M. S. Gudiksen, D. L. Wang, and C. M. Lieber, *Nature*, **420**, 57 (2002).
9. M. S. Hu, H. L. Chen, C. H. Shen, L. S. Hong, B. R. Huang, K. H. Chen, and L. C. Chen, *Nat. Mater.*, **5**, 102 (2006).
10. Y. J. Wu, C. H. Hsieh, P. H. Chen, J. Y. Li, L. J. Chou, and L. J. Chen, *ACS Nano*, **4**, 1393 (2010).
11. V. Pardo-Yissar, R. Gabai, A. N. Shipway, T. Bourenko, and I. Willner, *Adv. Mater.*, **13**, 1320 (2001).
12. T. W. Kim, D. C. Choo, J. H. Shim, and S. O. Kang, *Appl. Phys. Lett.*, **80**, 2168 (2002).
13. Y. Li, C. H. Ye, X. S. Fang, L. Yang, Y. H. Xiao, and L. Zhang, *Nanotechnology*, **16**, 501 (2005).
14. T. Y. Zhai, Z. J. Gu, Y. Dong, H. Z. Zhong, Y. Ma, H. B. Fu, Y. F. Li, and J. N. J. Yao, *Phys. Chem. C*, **111**, 11604 (2007).
15. D. Moore, J. R. Morber, R. L. Snyder, and Z. S. Wang, *Phys. Chem.*, **112**, 2895 (2008).
16. T. W. Kim, J. W. Shin, J. Y. Lee, J. H. Jung, J. W. Lee, W. K. Choi, and S. Jin, *Appl. Phys. Lett.*, **90**, 051915 (2007).
17. J. W. Shin, J. Y. Lee, Y. S. No, T. W. Kim, W. K. Choi, and S. Jin, *Nanotechnology*, **19**, 295303 (2008).
18. S. H. Cho, H. M. Andersson, S. R. White, N. R. Scttos, P. V. Brun, *Adv. Mater.*, **18**, 997 (2006)
19. M. W. Keller, S. R. White and N. R. Sottos, *Polymer*, **49**, 3136 (2008)
20. M. W. Keller, S. R. White and N. R. Sottos, *Adv. Func. Mater.*, **17**, 2399 (2009)
21. D. Li, Y. Wang, and Y. Xia, *Adv. Mater.*, **16**, 361 (2004).
22. A. Schroedter, H. Weller, R. Eritja, W. E. Ford, and J. M. Wessels, *Nano Lett.*, **2**, 1363 (2002).
23. W. E. Toe and S. Ramakrishna, *Nanotechnology*, **17**, R89 (2006).
24. B. C. Lee, Y. U. Jeong, S. O. Cho, J. Lee, S. Miginsky and G. Kulipanov, *Nucl. Instrum. Meth. B.*, **429**, 352 (1999)
25. A. Greiner and J. H. Wendorff, *Angew. Chem.-Int. Edit.*, **46**, 5670 (2007).
26. R. F. Egerton, P. Li, and M. Malac, *Micron*, **35**, 399 (2004).
27. J. Yuan, X. Liu, O. Akbulut, J. Hu, S. L. Suib, J. Kong, and F. Stellacci, *Nature Nanotech.*, **3**, 332 (2008)
28. C. H. P. Lupis, *Chemical Thermodynamics of Materials* (North-Holland, New York, 1983), Vol. 1, p. 134.
29. T. B. Reed, *Free Energy of Formation of Binary Compounds* (MIT, Cambridge, 1971), Vol. 1, pp. 7–9.
30. R. Souda, *Phys. Rev. Lett.*, **82**, 1570 (1999).
31. H. Hosono, H. Kawazoe, and N. Matsunami, *Phys. Rev. Lett.*, **80**, 317 (1998).
32. H. Guo, W. Maus-Friedrichs, and V. Kempter, *J. Appl. Phys.*, **86**, 2337 (1999).
33. C. Cannas, M. Mainas, A. Musinu, and G. Piccaluga, *Compos. Sci. Technol.*, **63**, 1187 (2003).